

Article

Open Source Multi-Head 3D Printer for Polymer-Metal Composite Component Manufacturing

John J. Laureto ¹ and **Joshua M. Pearce** ^{1,2,*}

¹ Department of Materials Science and Engineering, Michigan Technological University, 601 M&M Building, 1400 Townsend Drive, Houghton, MI 49931-1295, USA; jjlauret@mtu.edu

² Department of Electrical & Computer Engineering, Michigan Technological University, 121 EERC Building, 1400 Townsend Drive, Houghton, MI 49931-1295, USA

* Correspondence: pearce@mtu.edu; Tel.: +01-906-487-1466

Academic Editors: Salvatore Brischetto, Paolo Maggiore and Carlo Giovanni Ferro

Received: 1 March 2017; Accepted: 18 April 2017; Published: 15 June 2017

Abstract: As low-cost desktop 3D printing is now dominated by free and open source self-replicating rapid prototype (RepRap) derivatives, there is an intense interest in extending the scope of potential applications to manufacturing. This study describes a manufacturing technology that enables a constrained set of polymer-metal composite components. This paper provides (1) free and open source hardware and (2) software for printing systems that achieves metal wire embedment into a polymer matrix 3D-printed part via a novel weaving and wrapping method using (3) OpenSCAD and parametric coding for customized g-code commands. Composite parts are evaluated from the technical viability of manufacturing and quality. The results show that utilizing a multi-polymer head system for multi-component manufacturing reduces manufacturing time and reduces the embodied energy of manufacturing. Finally, it is concluded that an open source software and hardware tool chain can provide low-cost industrial manufacturing of complex metal-polymer composite-based products.

Keywords: open source; 3D printing; RepRap; composite; manufacturing

1. Introduction

The increased utilization [1,2] of self-replicating rapid prototyper (RepRap) 3D printers [3,4] using fused filament fabrication (FFF) (material extrusions by ASTM F2792-12a: Standard Terminology for Additive Manufacturing Technologies) [5] has increased the engineering applications of polymer extrusion materials. Printable polymer material characterization has increased the knowledge available to engineers for common PLA and ABS materials [6–9] along with an increasing list of thermoplastics [10,11], polymer metal composite materials [12–14] and polymer ceramic composite materials [15–18] for a number of novel applications, including medical and health-related components [19–23]. Subsequently, advancements in material understanding has led to the development of more sophisticated RepRap machines. Currently, multi-head printers (typically two hot ends) are readily available from re:3D, Aleph Objects, Prusa Research and other open source 3D printer manufacturers, and distributed designs are downloadable with creative commons and GPL licenses from the RepRap wiki and Internet repositories of 3D designs. Multi-head printers allow for multi-color printing to achieve aesthetic requirements and/or multi-material manufacturing of the same work piece [24]. Commonly, a sacrificial material (e.g., polyvinyl alcohol) is utilized as a supporting material to be easily removed during post-processing [25]. Recently, Ma et al. developed processing techniques to manufacture heterogeneous structures/composites using thin wall mold cavities and reusable multipart molds by combining shape deposition manufacturing (SDM), FFF and casting [26]. Furthermore, while still in the early stages of development, metal printing RepRap's provide a partial step towards full adoption of additive manufacturing techniques [27] and multi-material selection

in 3D manufacturing [28–32] to accommodate future requirements of material quality, design for manufacturing, processing monitor and achievement of near net shape [33]. Further expanding the RepRap machine customization is the advent of Franklin [34], an open-source 3D printing control software. Franklin's application to a variety of RepRap applications has been shown including: laser welding of HDPE polymer sheet [35], multi-material additive and subtractive fabrication [36], printed components for small organic farms [37] and voltage monitoring of a GMAW (gas metal arc welding) metal-based RepRap Delta printer [38]. Multi-material 3-D printers including those able to fabricate with composite materials such as fiber-reinforced polymer materials have been academically researched by Quan et al. [39]. Furthermore, similar to the application to be described are numerous applications of metal wire embedment into a primarily polymer matrix [40]. Recent investigative research has provided insight to copper wire encapsulation of copper for electronic sensing [41], tool path planning for wire embedment on FFF printed curved surfaces [42], metal fiber encapsulation for electromechanical robotic components [43], flexible printed circuit boards (PCB) for structural electronic devices [44] and open-source 3D printing CAD/CAM software for quality function deployment (QFD) and theory of inventive problem solving (TRIZ) optimization [45].

To further the scope of potential applications of RepRap manufacturing, this paper aims to describe a manufacturing technology that accomplishes a partial step forward to true multi-material selection. This paper provides free and open source hardware and software for printing systems that achieves metal wire embedment into a polymer matrix 3D printed part via weaving and wrapping procedures. In addition, a method utilizing OpenSCAD and parametric coding is provided that enables customized g-code commands to be developed for a given component design and material selection. Then, upon fixture placement, this method enables weaving and wrapping procedures by g-code line entries after each successive polymer layer deposition to create metal matrix composites. These composite parts are then evaluated from the technical viability of manufacturing and quality. Specifically, to identify the advantages of utilizing a multi-polymer head system for multi-component manufacturing, time studies are to be conducted and compared to traditional single-head per material manufacture of the same part. In addition, the metal/polymer interface bond strength is quantified with a burst pressure measurement. The results are presented and discussed in the context of low-cost distributed manufacturing of complex metal-polymer composites.

2. Materials and Methods

2.1. Fabrication of the Gigabot for Multi-Head Metal-Polymer Composite Printing

A re:3D Gigabot 3.0 3D printer [46] was modified for the development of the metal polymer matrix apparatus. The printing system utilizes a gantry system to accommodate five extruder nozzles and x-axis directional commands. A single NEMA 17 stepper motor with 20 tooth GT2 pulleys controls the movement of the x-axis. The y-axis commands are controlled by two NEMA 17s, one at each end of the gantry length. Similar to the y-axis, the z-axis movement is controlled by two NEMA 17s at opposite sides of the 60 cm × 60 cm (XY) build platform. Both z-axis and y-axis commands are sent to a NEMA 17 and replicated by the “follower” second motor based on the provided g-code. The printer is constructed with 80-20 extruded aluminum with bolts, nuts, fittings, threaded rods and brackets where required following the re:3D standard design. Figure 1 pictorially describes the printing apparatus to be discussed. Described are the relative locations of extruder/directional motors along with hot end locations on the x-axis gantry and electrical control board mounting locations.

Plastic 3D-printed components needed for the assembly are shown in Table 1. They were obtained through Thingiverse, a collaborative online maker space with downloadable component files (indicated by thing number in Table 1) or custom designed in OpenSCAD [47], a parameter modeling computer-aided design (CAD) software. Designed or downloaded part files were printed with polylactic acid (PLA) on either a MOST delta RepRap or a Lulzbot 5.0. Component design, coding and printing parameters allowed for easy modification, development, decreased print time and economical

use of filament material. All part files (.scad/STL) (Table 1) designed by MOST in OpenSCAD are available for download [48] under the GNU GPLv3 [49]. Secondly, the complete bill of materials including metric type accessory components and electrical components is displayed in Tables 2 and 3, respectively. Operational and installation instructions are available online at Appropedia [50].

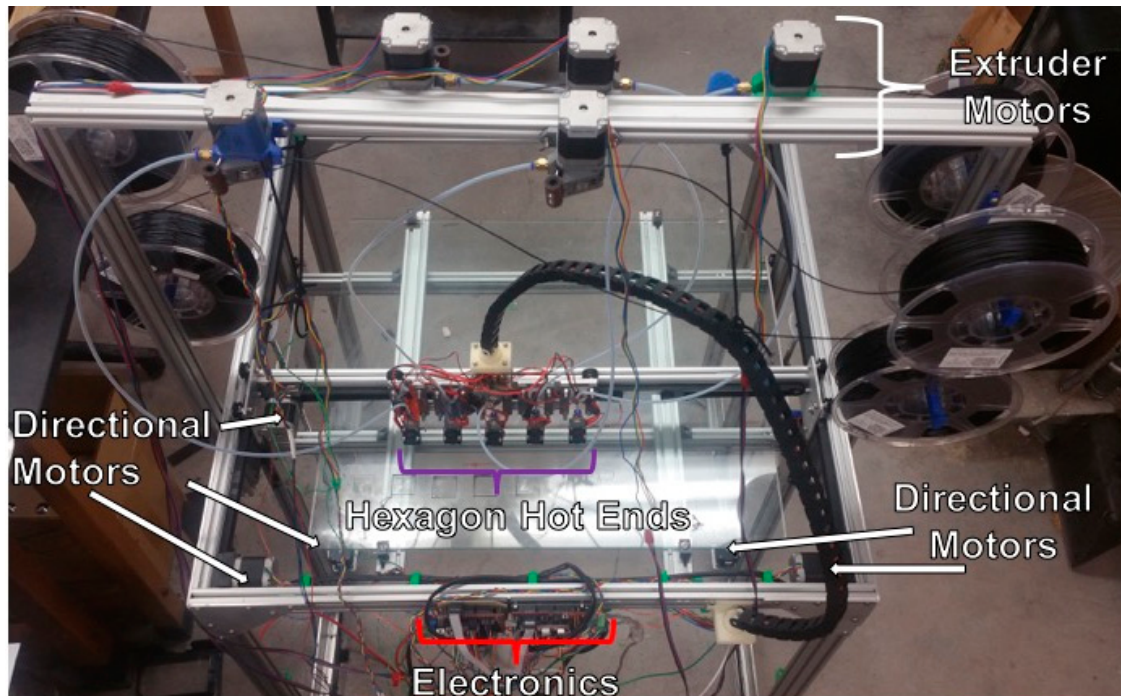


Figure 1. Complete manufactured metal-polymer composite Gigabot. Primary electromechanical components and their respective mounting locations are identified.

Table 1. Metal-polymer composite Gigabot printed/structural components.

| Part Name/Description | Count | Rendered Image | Part Name/Description | Count | Rendered Image |
|---------------------------------------|-------|----------------|----------------------------------|-------|----------------|
| Extruder Mount Bracket | 5 | | z-Height End Stop Solenoid Mount | 2 | |
| z-Height Bed Leveling Adjustment | 5 | | 80-20 Wire Guides | 10 | |
| z-Height Bed Leveling Dovetail Mounts | 5 | | Gantry Cable Supports | 3 | |
| Filament Spool Holders thing:1269563 | 6 | | Build Plate Fixturing Brackets | 4 | |
| 80-20 M4 T-Slot Mount thing:1061769 | 2 | | Hexagon Hot end Fan Mount | 5 | |

Table 1. Cont.

| Part Name/Description | Count | Rendered Image | Part Name/Description | Count | Rendered Image |
|--|-------|----------------|--------------------------------------|-------|----------------|
| z-Height Z1 and Z0 Leveling Screw Knob | 2 | | MOST Bowden Extruder Drive | 5 | |
| Gantry Mount Cable Carrier Connection | 1 | | Arduino Mega 250 Mount Bracket | 1 | |
| Customized I/O Board Mount Bracket | 1 | | 80-20 Cable Carrier Mount | 1 | |
| Gantry Mount Electrical Connection Board | 1 | | y-Carriage Belt Clamp | 2 | |
| y-Axis End Stop Solenoid Mount | 2 | | Compact Bowden Extruder thing:275593 | 1 | |

Table 2. Metal-polymer composite Gigabot mechanical bill of materials.

| Part Description | Count | Source | Serial/Pat Number |
|---|----------|---------------------------------|-------------------|
| GT2 3MR 9-mm Wide GT2 Timing Pulley | 1(15 ft) | Gates | - |
| 9-mm Idler Pulley with 625-2RS Bearings | 3 | Gates | - |
| M5x8 Button Head Cap Screws | 100 | re:3D | - |
| Hexagon Full Metal Hot-End 1.75 mm, 12 V | 5 | BoltDepot.com | - |
| Cyclemore 1.0-mm Brass Nozzle | 5 | IC3D-Hexagon | X000SV0T0N |
| PC4-M6 Push-In Fitting | 10 | Cyclemore | X000WJAXH5 |
| 53 Link Cable Carrier | 1 | Cyclemore | 30-60007-016-FBA |
| Teflon (PTFE) Bowden Tube 1.75 mm (2.0 mm ID/4.0 mm OD) | 25 ft | Re:3D | - |
| 3/8"-8 ACME Threaded Rods | 2 | 3D CAM | BOWDEN2M |
| V-Grove Roller Bearings | 20 | re:3D | - |
| 67 mm × 60 mm Annealed Glass Build Plate | 1 | Re:3D | - |
| 80-20 Series 20 T-Slot Nuts | 100 | Locally sourced | - |
| Threaded Rod Z-Nut Cup | 2 | re:3D | - |
| MXL 18 Tooth Motor Pulley | 2 | re:3D | - |
| MXL 36 Tooth Motor Pulley (Threaded Rod) | 2 | re:3D | - |
| z-Axis MXL Belt | 2 | re:3D | - |
| Aluminum Side Plate | 4 | re:3D | - |
| Aluminum Corner Plate | 8 | re:3D | - |
| Rectangular Brackets for Extruder Motor Gantry | 2 | re:3D | - |
| 3 mm × 9 mm Stainless 18-8 Washer | 100 | BoltDepot.com | 7319 |
| DIY: Gigabot Parts Kit | 1 | re:3D | - |
| M2 Hex Nut | 100 | BoltDepot.com | - |
| Eccentric Wheel Spacer | 4 | re:3D | - |
| Z-Motor Shelf | 2 | re:3D | - |
| Truck Plates (L/R) | 2 | re:3D | - |
| Thermal Tape | 10 | adafruit | 1468 |
| A4988 Pololu Heat Sink | 10 | Pololu Robotics and Electronics | - |

Table 3. Metal-polymer composite Gigabot electrical components.

| Part Description | Count | Source |
|----------------------------------|-------|--------|
| NEMA 17 Stepper Motor | 10 | - |
| RAMPS 1.4 | 2 | - |
| A4988 Pololu Driver | 10 | - |
| Arduino 250 Mega | 1 | - |
| Custom I/O Board | 1 | - |
| 12 V Power Supply | 1 | - |
| 36 V Power Supply | 1 | - |
| End Stop Solenoid Limit Switches | 5 | re:3D |

The x-axis gantry is installed with five full metal 1.75-mm hexagon hot ends [51] spaced 55 mm apart. Spacing of the hot-end is controlled by two manufactured aluminum plate measuring 3.175 mm × 25.400 mm × 295.75 mm. The 55mm spacing is driven by the placement of the z- leveling dovetail mounting points. The aluminum plates and z-leveling dovetails are fixtured by the application of M5 bolts and roller bearings. The printed hexagon mounting fixture is a tongue and groove design allowing for independent z-axis leveling with adjustment of an M3 set screw, i.e., each extruder nozzle is individually leveled to the build platform. This allows for replicate parts to be simultaneously printed assuming that gcode commands do no exceed the 55mm spacing machine constraint. Figure 2 displays the x-gantry mounting system.



Figure 2. X-axis gantry assembly. 5× Hexagon Full-Metal 12 V hot ends are shown fixtured to their respective 'Z-Height Bed Leveling Adjustment' part files. As shown, dovetail leveling mechanisms are attached to the machined aluminum plate (3.175 mm × 25.4 mm × 295.75 mm) with Hexagon nozzle diameter cylindrical axis spaced 55 mm.

The five hexagon hot ends are provided filament through Bowden sheaths constructed from 4 mm OD (2 mm ID) pressure fitting compatible polytetrafluoroethylene (PTFE) flexible tubing. The Bowden extruder system decreases the weight on the x-axis gantry, thus allowing for faster and more accurate prints. Decreased weight on the x-axis gantry is also advantageous, as it will decrease the likely hood of the single x-axis NEMA 17 skipping, leading to a loss of positioning. The Bowden extruder bodies, NEMA 17s and assembly structures are mounted to the secondary elevated gantry. M5 and t-slot nuts allow proper fixture to the secondary 80–20 aluminum gantry. Figure 3 provides further details of the five extruder motors installed on the gantry along with a close up image of the extruder motor assembly. Furthermore, the feed filament is spooled adjacent to its respective extruder motor.

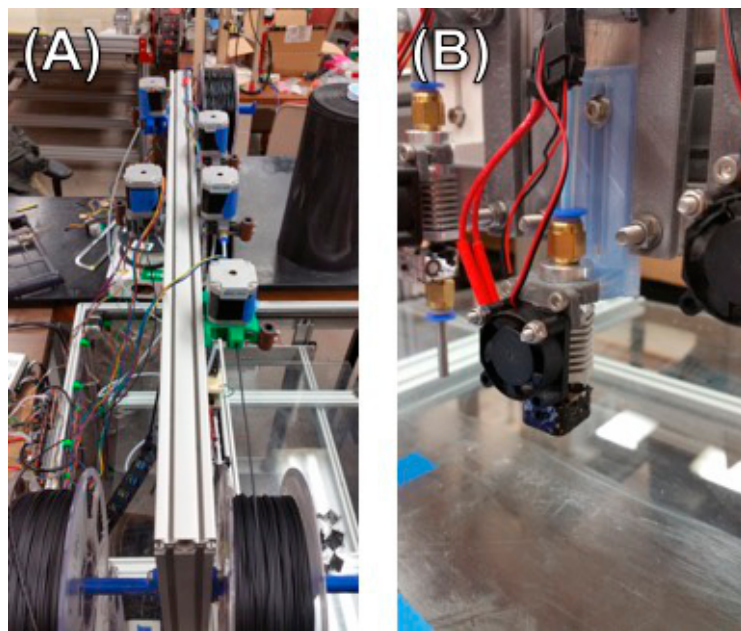


Figure 3. (A) Top printer gantry with fixtured 5 NEMA 17 extruder drive motors and respective “MOST Bowden Extruder Drive” printed components; (B) hexagon hot-end assembly detail with “Z-Height Bed Leveling Adjustment” dovetails.

Additionally, due to the large build platform, two z-axis zeroing locations are utilized. Two M5 screws with fitted ergonomic adjustment knobs and tension springs allow for z-axis leveling independently. Upon proper adjustment, the x-axis gantry extruders can be leveled to the build platform. Figure 4 displays the leveling system.

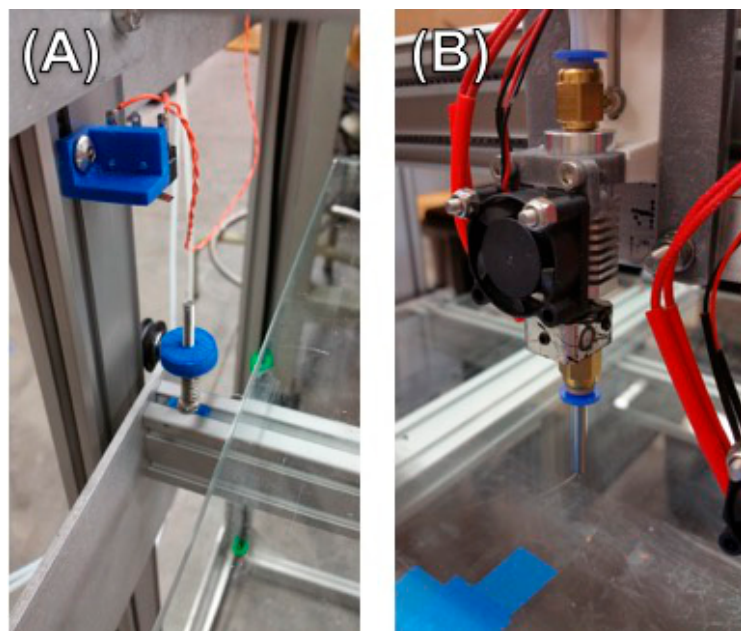


Figure 4. (A) Bed platform Z-height leveling. Shown are “Z-Height End Stop Solenoid Mount”, “80-20 M4 T-Slot Mount thing: 1061769” and “Z-Height Z1 and Z0 Leveling Screw Knob” fixtured to 80-20 aluminum rails with M5 nuts; (B) height adjustment assembly shown at the maximum height adjustment in contrast to Figure 3B.

2.2. Circuit Assembly and Printer Control

To accommodate the quantity of NEMA 17 stepper motors, solenoid end stops and thermistors, a custom circuit board enabling the application of two RAMPS (RepRap Arduino Mega Pololu Shield) 1.4 is created [52]. Application of this circuit, as described in Figures 5 and 6, provides two functional RAMPS 1.4 and subsequent A4988 stepper motor driver carriers [53] from one Arduino Mega 2560 [54]. The KiCad-PcbNew 4.0.3 designed I/O board communicates with the secondary RAMPS 1.4 board allowing for the further allocation of pins on the Arduino microcontroller [55]. Pin assignments, as presented in the Franklin printer profile, are shown in Tables 4 and 5. The A4988 potentiometers are adjusted to provide 0.6–1.2 mV of potential measured between ground. Each potentiometer is fitted with an aluminum heatsink fixture with thermal tape to aid in temperature control.

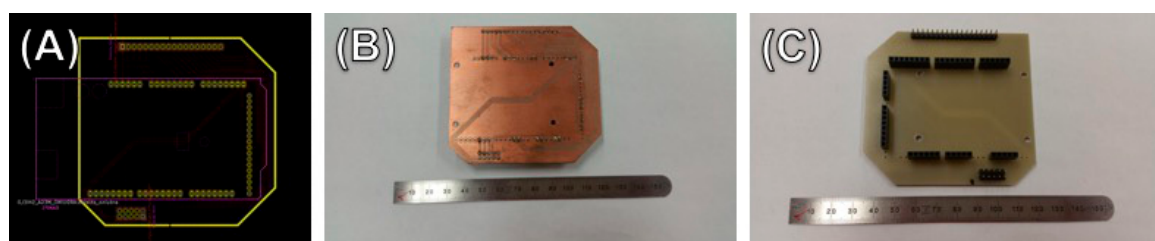


Figure 5. (A) Electrical diagram/schematic developed in KiCAD-PcbNew; (B) milled PCB surface for representation; (C) PCB pin side for representation.



Figure 6. Assembled two RAMPS 1.4 with custom I/O PCB per the KiCAD-PcbNew specification.

Table 4. Stepper motor pin assignments ¹.

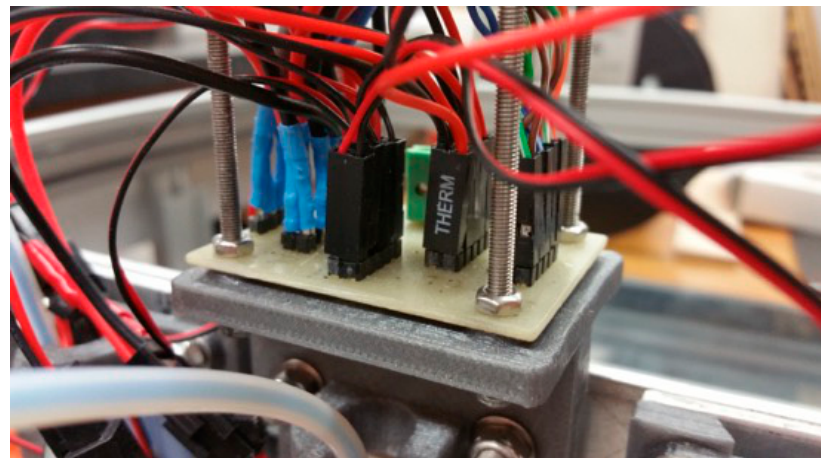
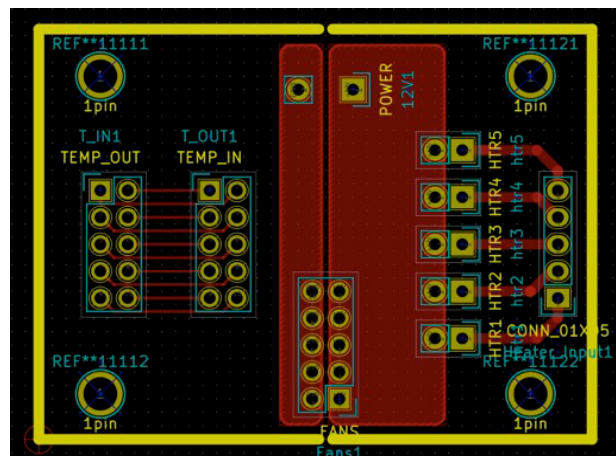
| Pin Type | X _D | Y _{0D} | Y _{1D} | Z _{0D} | Z _{1D} | Ex _{0E} | Ex _{1E} | Ex _{2E} | Ex _{3E} | A _E |
|-----------|----------------|-----------------|-----------------|-----------------|-----------------|------------------|------------------|------------------|------------------|----------------|
| Step | D32 | D60(A6) | D43 | D46 | D37 | D29 | D36 | D26 | D54(A0) | D35 |
| Direction | D47 | D61(A7) | D41 | D48 | D39 | D31 | D34 | D28 | D55(A1) | D33 |
| Enable | D45 | D56(A2) | D45 | D62(A8) | D45 | D45 | D30 | D24 | D38 | D45 |
| Min Limit | D3 | D14 | D23 | D18 | D0 | D0 | D0 | D0 | D0 | D0 |
| Max Limit | D2 | D15 | D25 | D19 | D0 | D0 | D0 | D0 | D0 | D0 |

¹ Pin assignments are relative to the A4988 and stepper motors physical location on the RAMPS 1.4. Refer to Figure 5 for specific location details.

As indicated in Table 5, 24-V heater cartridges, cooling fans and thermistors are connect to their respective RAMPS 1.4 positions through a secondary custom I/O board. The I/O board acts as a central hub for all communication to the components on the x-axis gantry. Figure 7 identifies the location of this board and the connection points of each component, while Figure 8 describes the PCB in greater detail.

Table 5. Hexagon hot end Arduino pin assignments.

| Pin Type | Ex0_E | Ex1_E | Ex2_E | Ex3_E | A_E |
|------------|----------------|----------------|----------------|----------------|----------|
| Heater | D9 | D10 | D42 | D64(A11) | D8 |
| Fan | D0 | D0 | D0 | D0 | D0 |
| Thermistor | A14(D68) | A15(D69) | A10(D64) | A12(D66) | A13(D67) |

**Figure 7.** Assembled secondary I/O PCB for x-axis gantry components.**Figure 8.** Secondary I/O PCB schematic developed in KiCAD-PcBNew. Connection zones as indicated in this image are further indicated in Figure 7 as previously described.

The metal-polymer composite Gigabot requires two power supplies to meet full operational requirements. As designed, an input 110/220 V, output 12 V 20 A power supply is utilized for thermistor operation. An input: 110/220 V, output: 36 V 10 A power supply enables the operation of both RAMPS 1.4 boards and the secondary custom I/O board. Thus, location, position and extruder motor(s) operate on a separate power supply as compared to the thermistors and heater cartridges.

In total, ten NEMA 17 motors need to be controlled for proper functionality of the printer assembly. Specifically, there is a NEMA 17 assigned to each movement axis as listed; X, Y0, Y1, Z0, Z1, E0, E1, E2, E3 and A. Further functional description of each motor is shown in Table 6 along with a qualitative electromechanical process map, shown in Figure 9, indicating primary connection mechanisms' hot ends, thermistors, heater cartridges, end stops, extruder motors and directional motors.

Table 6. NEMA 17 motor settings and physical description.

| Motor (x_D = direction, x_e = extruder) | Coupling (steps/mm) | Limit Velocity (mm/s) | Limit Acceleration (mm^2/s) |
|--|---------------------|-----------------------|---|
| X_D | 59.292 | 150 | 250 |
| $Y0_D$ | 59.292 | 150 | 250 |
| $Y1_D$ | 59.292 | 150 | 250 |
| $Z0_D$ | 2133.333 | 4 | 250 |
| $Z1_D$ | 2133.333 | 4 | 250 |
| $Ex0_E$ | 100 | 200 | 1000 |
| $Ex1_E$ | 100 | 200 | 1000 |
| $Ex2_E$ | 100 | 200 | 1000 |
| $Ex3_E$ | 100 | 200 | 1000 |
| A_E | 100 | 200 | 1000 |

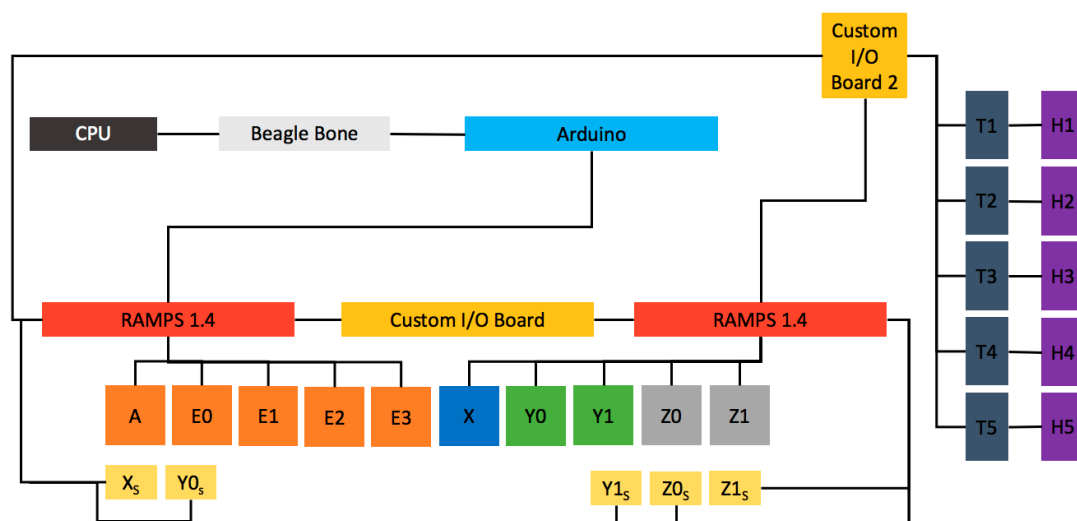


Figure 9. Electromechanical process map of the metal-polymer composite Gigabot. This diagram represents a qualitative understanding of the primary connection points between operational mechanisms and electronic controllers. Extruder motors: A, E0, E1, E2, E3. Directional motors: X, Y0, Y1, Z0, Z1. Solenoid end stops: X_s, Y0_s, Y1_s, Z0_s, Z1_s. Thermistors: T1, T2, T3, T4, T5. Heater cartridges: H1, H2, H3, H4, H5.

The open-source firmware (Franklin) controls the motion of the printer assembly. The graphic user interface (GUI) of Franklin provides the user with an interface in which to upload g-code and customize printer settings and parameters. g-code and printer settings are communicated to the printer through the host computer into the controller. Respective g-code is formulated upon the generation of a stereolithography file (e.g., STL file). Print layer g-code was developed with Slic3r 1.2.9 [56]. The resultant g-code is typical such that the application into any RepRap printer should be easily achieved. Unique, however, is the metal-polymer composite Gigabot's multiple motors per axis (e.g., Y0/Y1, Z0/Z1 and Ex0/Ex1/Ex2/Ex3). In the current state, Slic3r is unable to individually command multiple extruders and axis motors simultaneously. Subsequently, Franklin allows for motors to be controlled via a "leader and follower" principle. For example, a printer controlled by Franklin a g-code command of "G1 Y213 Z55" will signal movement of Y0/Y1 and Z0/Z1 to a relative position of 213 mm and 55 mm, respectively. In effect, the g-code command pulsed through the controller to the stepper motor is initially recognized by the "leader" (i.e., Y0 or Z0 and henceforth followed and/or replicated by Y1 or Z1). The resultant interaction is duplicate movements by the affected stepper motors. The "leader and follower" principle are also used for the Ex0E-Ex3E extruder motors (i.e., four of the five hot ends will extrude the same portion of filament based on a standard g-code

command). In this circumstance, Ex0E is the leader extruder followed by Ex1E, Ex2E and Ex3E. Unique to the metal-polymer composite Gigabot machine is extruder AE. Functionally, AE, is a directional movement axis, which has been modified to be used as an extruder. The proper coupling, limit velocity and acceleration settings in Franklin allow for this change. Separation of AE from Ex0E–Ex3E allows for individualized commands within the g-code. Other than “E” commands, Slic3r cannot currently generate extruder commands for different extruders. To introduce “A” commands, visual basic applications were utilized to reformat the text of the outputted g-code. Table 7 describes a sample operation of this process.

Table 7. Visual Basic g-code modifier (spreadsheet reference cell#).

| | Initial g-code Command Line | G1 F900 X143.487 Y114.988 E0.51434 (A27) |
|--------------------|--|---|
| Operation 1 | =IF(ISNUMBER(SEARCH("G1",A27)),RIGHT(A27,LEN(A27)-SEARCH("E",A27,1)+1),"NA") | E0.51434 |
| Operation 2 | =IF(ISNUMBER(SEARCH("G1",A27)),RIGHT(A27,LEN(A27)-SEARCH("E",A27,1)),"") | 0.51434(E27) |
| Operation 3 | =IF(ISNUMBER(SEARCH(" ",E27))," ","A") | A(F27) |
| Operation 4 | =CONCATENATE(F27,E27) | A0.51434(G27) |
| Operation 5 | =IFERROR(IF(ISNUMBER(SEARCH(" ",G27)),A27,CONCATENATE(A27&" "&G27)),A27) | G1 F900 X143.487 Y114.988 E.51434 A0.51434 |

The process described in Table 7 is for the utilization of all five hot ends for replicate polymer component printing. However, there are applications in which AE may be used independently relative to Ex0E–Ex3E. In these unique circumstances, g-code for AE is made separately and then superimposed on the g-code for Ex0E–Ex3E, resulting in a composite g-code.

2.3. Modification of Extruder A_E for Wire-Feeding

A modified Bowden extruder design (thing: 275593) was utilized for a wire feeding/guide apparatus. The print assembly and miscellaneous hardware were assembled in a standard manner; however, the MK7 drive gear was inverted. Inversion of the MK7 drive gears allows for a smooth, non-galled, surface to contact the metal wire. Electrical tape surface coatings were applied to both the 608zz idler bearing and the smooth end of the MK7 drive gear for the grip of a wire. The feed wire spool is mounted near the wire extruder such that the top dead center is tangent to the primary axis of the Bowden feed pathway. Figure 10 displays the assembled metal wire feeder. Utilizing the same Bowden sheath as would a polymer filament, an 1100 series aluminum wire with a diameter of $0.508\text{ mm} \pm 0.012\text{ mm}$ is directed down through a Hexagon hot end. In a modified application such as this, the hexagon hot end nozzle has been removed while the main assembly is present to help guide the wire. A M5 pressure fitting, similar to those in the Bowden sheath assembly, is mounted to the hot end in replacement of the 1.0-mm nozzle. The utilized pressuring fitting allows for installation of a 304 stainless tube with an outer-diameter (OD) of 1.422 mm, (-0.050 mm to $+0.101\text{ mm}$) and inner-diameter (ID) of 2.184 mm. The outer diameter is equivalent to a standard 4 mm (OD) and secures properly into a M5 pressure fitting. The ID is substantial enough to allow for passage of the 0.508 mm diameter wire while also providing room for a PTFE fitting to decrease wire friction while the wire exits the tube. The wire feed guide tube and remaining extruders (Ex0E–Ex3E) are run simultaneously. Thus, the 304 tubing prior to installation in the pressure fitting is cut to a length of ~46 mm. Thus, all extruder nozzles and wire guide tubes can be leveled to the build platform at a similar height. Figure 11 displays the assembly of the structure.

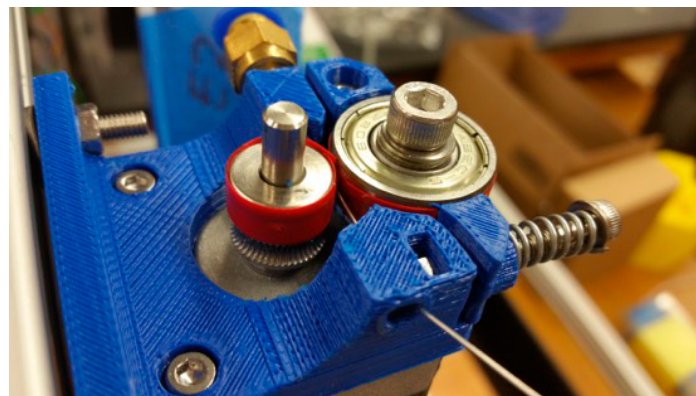


Figure 10. Wire feed Bowden assembly assembled with supplementary hardware and “Compact Bowden Extruder thing: 275593”. Note that a common 1.75 mm extruder drive tooth gear has been inverted and coupled with electrical tape to provide frictional rolling resistance to aid in guiding the 1100 series aluminum wire.



Figure 11. Wire feed guide tube. As shown, a standard M6 4.0 mm press fitting accommodates the standard threading in the hot-zone of a standard hexagon 12 V hot end. 304 stainless tubing press fits similar to a 4.0 mm PTFE tubing. Scrap PTFE tubing is fixtured to the exit zone of the 304 stainless tubing to reduce the friction associated with wire wrapping processes.

The wire feed Bowden assembly enables the ability for small increments (e.g., 1–10 mm) of wire feeding based on an AE g-code command. However, the drive mechanism is not primarily responsible for the displacement of aluminum wire. In practice, an initial length of wire is fed through the wire guide. The excess length is fixed to a pin located on the metal-polymer composite Gigabot’s build platform. Controlled movement of the wire feed cross head allows for accurate positioning of the aluminum wire. As shown in Figure 9, placement of multiple secondary pins will allow for wrapping of the aluminum wire. Positioning of the fixture on the build plate is critical to the success of the wrapping procedure. Secondary fixtures are independent of the metal-polymer composite Gigabot’s motor controllers; thus, offsets, in Slic3r, are to be programmed into resultant g-code. The offsets are readily determinable by manually progressing the wire-feed hot end to a known location on the secondary fixture and recording the positional coordinates provided by Franklin’s GUI. The deviation in positional coordinates between the known location on the secondary fixture and Franklin’s GUI output corresponds to the offsets required. In this application, positioning is only critical and programmable in the two-dimensional (XY) realm, as the z-axis, as mentioned earlier,

is adjusted mechanically by the operator. The primary g-code, responsible for the wire rapping operations, can be produced from a digital parametric model. In this method, the model is set up to accommodate the fixture as shown in Figure 12. For proper generation of both the fixture and parametric wrapping, the model must be modeled in the same relative positioning. In these analyses, OpenSCAD modeling was used to model the entire print pre-production. Figure 13 displays a rendering of the OpenSCAD modeling.

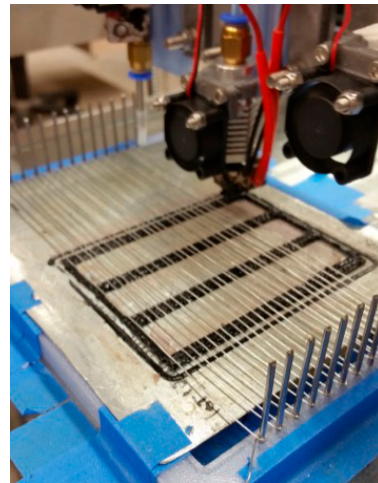


Figure 12. In situ process photo of Franklin-controlled wire wrapping.

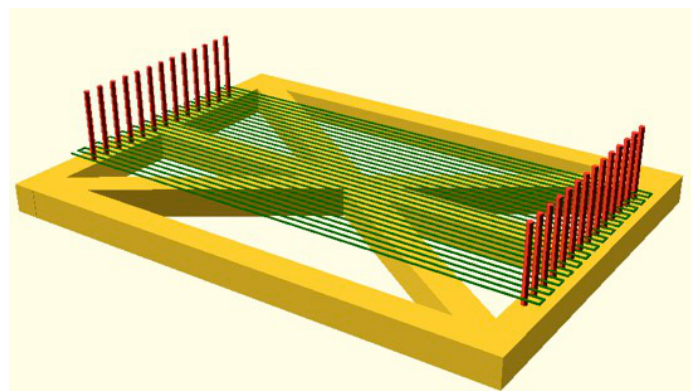


Figure 13. Rendering of parametric OpenSCAD model (yellow: fixture; red: pins; green: wire). In situ process of the designed OpenSCAD model displayed in Figure 12.

g-code generated for the wire weaving is obtained by individually exporting the (green) wire portion as an STL. The exported model can be placed into Slic3r and sliced into a single layer forgoing any Z-components. The fixture, pins and wire modeling in OpenSCAD all share an equivalent “zero” position. Thus, assuming that a specific location on the fixture can be located, the required offsets to realign the digital wire model to the physical fixture can be obtained. Typically, modifications to the generated wire wrapping g-code are required, as the models shown in Figure 11 are designed to a nominal dimension. Thus, no tolerance is designed for accommodating manufacturing/assembly of fixture positioning issues. The total realized errors, due to assembly accuracy, are not realized until initial test prints begin.

2.4. Composite Printing—Utilizing Wire-Feed Guide and Standard Brass 1.0 mm Extruder Nozzle

Slic3r 1.2.9 allows for the placement of custom g-code before and/or after a layer has been completed. Application of this software utility allows for customized wire weaving operations to occur during a standard print operation. Thus, composite structures containing 1100 series aluminum wire along with polymer FFF materials are realized. Developed processing parameters, metal-polymer composite printer modifications are all in an effort to accommodate pre-prescribed models relative to the funding agency project scope. Further secondary operations during printing are required. For example, the aluminum wires need to be heated to an elevated temperature such that the localized polymer material, at each intersection, is melted. Currently, a heater is utilized to elevate the local temperature of the metal/polymer interface. The localized heating enables the 1100 series aluminum wire and polymer material to bond sufficiently and provide significant z-height clearance for the subsequent layers of polymer material.

2.5. Polymer Filament Material Selection and Printing Parameter Development

Readily available polymer materials polyethylene terephthalate glycol modified (PETG) and polypropylene (PP) were selected for analysis. PETG was sourced from Shenzhen Esun Industries Co., Ltd. (eSUN, Shenzhen, China) and the PP from Gizmo Dorks (Temple City, USA). Materials were procured in 1 kg filament spools with a nominal diameter $1.75\text{ mm} \pm 0.05\text{ mm}$ where roundness tolerances were not considered. Relevant intrinsic materials properties, as described by the respective materials' technical data sheets, are displayed in Table 8 [57,58].

Table 8. Material properties of PETG and PP.

| - | eSUN PETG | Gizmo Dorks PP ¹ |
|------------------------------|------------|-----------------------------|
| Print Temperature (°C) | 230–250 | 230–260 |
| Build Plate Temperature (°C) | 80 or none | 60 |
| Feeding Speed (mm/s) | 30–80 | 90 |

¹ Gizmo Dorks presents further and more detailed parameter settings beyond those presented here.

A variety of experimental trial prints and manufacturing runs were conducted to optimize the printing parameters. The primary metrics considered include: print speed (mm/s), extrusion/hot end temperature (°C), layer height (mm), nozzle diameter (mm), shell thickness (mm) and bottom/top layer thickness (mm). An optimized parameter set yields a quality component upon visual inspection and can be quantified with interface adhesion. Developed parameter sets are discussed and further evaluated below.

2.6. Composite Printing Tests for Metal-Polymer Composite Gigabot

Test coupons were generated using OpenSCAD to dimensions of $25.4\text{ mm} \times 25.4\text{ mm} \times 25.4\text{ mm}$. The coupon geometry was selected to provide a simplistic volumetric model for which to compare print quality and to provide power consumption data. Print quality was determined by metrics quantifiable by visual inspection and digital caliper measurements ($\pm 0.01\text{ mm}$) (e.g., surface smoothness, dimensional accuracy and apparent layer adhesion). Dimensional adherence to the as-designed nominal dimension of the test coupon is deeply dependent on the sliced parameter set. The intent of the dimensional analysis is to quantify the part dimensional stability per extruder, not to determine the optimum parameter set to produce nominal and/or accurate components (i.e., $\pm 0.127\text{ mm}$). Energy consumption measurements were performed with a multi-meter for cumulative kWh monitor ($\pm 0.01\text{ kWh}$) and instantaneous power draw (Watts).

3. Results

3.1. Resultant Print Quality and Power Consumption Measurements

An example of the resultant polymer-metal composite structure is shown in Figure 14.



Figure 14. Metal polymer composite generation dimensionally accurate to prescribed models. Cross-flow media is 1100 series aluminum wire, encased in a polymeric matrix of PETG.

Resultant print quality is shown in Figure 15. A layer height of 0.5 mm was utilized in conjunction with a 1.0-mm brass nozzle. Evidence of the relatively large layer height and nozzle are shown on the component surfaces. Wave patterns apparent on the exterior perimeters of the test coupon(s) are the result of the twenty-five percent infill percentage parameter. Wave “peaks” are adjacent to vector pathways of the infill section lines on the interior surface of the perimeter. Dimensional measurements identifying deviation from nominal are shown in Table 9. Width, length and height correspond primarily to the x, y and z coordinates, respectively.



Figure 15. Printed component part quality (visual inspection) prior to removal from substrate to be measured for dimensional precision. As indicated in Table 9, dimensional variation between hot ends is determined to be a critical metric in contrast to print parameter adjustable deviation from nominal dimensional values (i.e., 25.4 mm).

Electrical power draw (Watts) for a variety of operating conditions is shown in Table 10. Conditions were selected to identify the power requirements for each component of the metal-polymer composite Gigabot, including thermistors, heater cartridges and stepper motors (extruder and position).

Table 9. Printed component average dimensions relative to nominal dimensions (\pm mm).

| Dimension | (A _E) | $\pm\sigma$ | (E0 _E) | $\pm\sigma$ | (E1 _E) | $\pm\sigma$ | (E2 _E) | $\pm\sigma$ | (E3 _E) | $\pm\sigma$ |
|-------------------------|-------------------|-------------|--------------------|-------------|--------------------|-------------|--------------------|-------------|--------------------|-------------|
| X (Width) ¹ | 25.82 | 0.08 | 25.86 | 0.08 | 25.93 | 0.06 | 25.94 | 0.06 | 25.93 | 0.18 |
| Y (Length) ¹ | 25.77 | 0.06 | 25.80 | 0.04 | 25.79 | 0.06 | 25.88 | 0.01 | 25.70 | 0.04 |
| Z (Height) ¹ | 26.42 | 0.09 | 26.66 | 0.05 | 26.39 | 0.06 | 26.45 | 0.04 | 26.25 | 0.03 |

¹ Nominal designed dimension of 25.4 mm. Averages determined from a sample size of three measurements.

Table 10. Power consumption for various metal-polymer composite Gigabot operating conditions (Watts).

| Operating Condition | Power Draw (Watts) ¹ |
|---|---------------------------------|
| 36 V 10 A Stand Alone | 5.9–6.9 |
| 12 V 20 A Stand Alone | 13.2–14.0 |
| 12 V 20 A with Heaters On | 117–118 |
| 12 V 20 A and 36 V 10 A with Heaters On | 138–144 |
| 12 V 20 A and 36 V 10 A Temp Limit (220 °C) | 138–144 |
| 12 V 20 A and 36 V 10 A with Motors Enabled | 45.9–46.7 |
| 12 V 20 A and 36 V 10 A with no Heaters or Motors | 21–22 |
| 12 V 20 A and 26 V 10 A Motors on Heaters on and Printing | 138–144 |

¹ Measurements are recorded in an enabled state, but idle condition, i.e., not performing a build sequence

Cumulative kWh, per print cycle, measurements are displayed in Table 11. Four parameter sets were utilized for this analysis utilizing the same test coupon geometry to quantify visual part quality. The four conditions were setup as follows: twenty-five percent infill \times 5 extruders, one-hundred percent infill \times 5 extruders, twenty-five percent infill \times 1 extruder and 100 percent infill \times 1 extruder. Single extruder studies used the A_E stepper motors and respective heater elements to print five test coupons. Conversely, multi-extruders utilized five extruders' replication the actions of A_E. The metal polymer composite Gigabot was allowed four minutes of heat up from 100 to 220 °C for each condition. All print cycles resulted in five printed components.

Table 11. Energy consumption (kWh) measurements for various print cycles.

| Conditions | Metrics | Heat Up | Build | Total kWh |
|---------------------------------------|----------------------------------|---------|---------|-----------|
| 25% In-Fill and \times 5 Extruders | Time (min) | 4 | 9 | 0.03 |
| | Cycle Power (Watts) ¹ | 140–144 | 138–144 | |
| 100% In-Fill and 5 \times Extruders | Time (min) | 4 | 20 | 0.06 |
| | Cycle Power (Watts) ¹ | 140–144 | 138–144 | |
| 25% In-Fill and 1 \times Extruders | Time (min) | 4 | 10 | 0.01 |
| | Cycle Power (Watts) ¹ | 68–69 | 62–65 | |
| 100% In-Fill and 1 \times Extruders | Time (min) | 4 | 21 | 0.03 |
| | Cycle Power (Watts) ¹ | 68–69 | 62–65 | |

¹ Table 10 measured values.

3.2. Printing Parameter and Material Development

Slic3r 1.2.9 was selected as the primary slicing tool for g-code generation. As compared to Cura 15.04.6, Slic3r allowed for custom g-code, including: start g-code, end g-code, before layer change g-code and after layer change g-code [59]. Without the implementation of this interface combining metal wire wrapping processes with the polymer, printing would not be possible.

PETG was selected as the primary polymer material for the metal/polymer composite over PP. In virgin filament form, PETG is rigid in comparison to PP. During manufacturing trials, PP would consistently twist and bend within the Bowden sheath, thus causing filament jams. Developing

processing techniques to ensure consistent material flow throughout the hot end was troublesome. Secondly, PP requires like to like material for proper build plate adhesion. Specifically, PP build plates are required to reduce delamination part warping after deposition. Conversely, PETG is readily suited to adequately bond to a glass build plate with the application of a thin adhesive layer from a glue stick. Due to the relative ease of manufacturing and build preparation setup, the advantages of PETG over PP are clear from a manufacturing standpoint.

Selected build parameters are displayed in Table 12. Determined build parameters are relative to a 1.0-mm hot end nozzle and should be modified as such in the case of any significant machine design change. Critical metrics are identified in Table 12. However, more elaborate and complete “.ini” files are included in the Supplementary Documentation.

Table 12. Manufacturing parameters for PETG on a metal-polymer composite Gigabot.

| Retraction Parameters Type | Corresponding Slic3r Setting |
|---------------------------------|------------------------------|
| Print Temperature (°C) | 220 |
| Print Speed (mm/s) | 40 |
| Layer Height (mm/s) | 0.5 |
| Horizontal Shells (Top) | 2 |
| Horizontal Shells (Bottom) | 3 |
| First Layer Extrusion Width (%) | 200 |
| Extrusion Multiplier | ×2 |

Without sufficient accommodation, PETG was noted to string during vector movements and stick to the nozzle. These phenomena caused concern in regards to dimensional stability, printed part accuracy and visual appearance of the printed component. Proper calibration of retention setting and seam locations was required. Table 13 identifies the required print parameter settings to ensure adequate retraction of PETG filament after a vector pass such that no undesired filament was deposited onto the printed part.

Table 13. Manufacturing parameters for PETG on a metal-polymer composite Gigabot.

| Parameters Type | Corresponding Slic3r Setting |
|--------------------------------------|------------------------------|
| Length (mm) | 10 |
| Lift Z (mm) | 0.5 |
| Speed (mm/s) | 100 |
| Extra length on restart (mm) | 8 |
| Minimum travel after retraction (mm) | 0.1 |
| Retract on layer change | Yes |
| Wipe while retracting | Yes |
| Seam position | Nearest |

4. Discussion

4.1. Practical Application of the Metal-Polymer Composite Gigabot

Attachment of ×5 extruder nozzles to a gantry allows for significant energy/part savings. The developed system contains nearly identical embodied energy and energy consumption when compared to other Cartesian type printer systems on the market (e.g., Lulzbot) [60]. Specifically, comparable systems use a near equivalent amount of NEMA 17 motors: one X-motor, one–two Y-motor(s) and two Z-motors. However, the metal-polymer composite Gigabot allows operators to utilize the embodied energy in the manufacture of multiple components in regards to all X, Y and Z travel movements in all ×5 nozzles simultaneously. Furthermore, the timed-based analysis presented in Section 3.1 displays significant manufacturing time variances between the parameter sets. Most notably are the advantages of utilizing the metal-polymer Gigabot for the manufacture

of $\times 5$ components. At 25% in-fill operators printing single components (i.e., one hot end) at a time, 70 min are required for complete manufacture, while 100% requires 125 min for manufacturing. Comparatively, utilizing the full capacity of the metal-polymer Gigabot reduces manufacturing time to 13 min and 24 min for 25% and 100% in-fill, respectively. On a percentage basis, this is a variance of ~438% and ~420% for 25% in-fill and 100% in-fill, respectively. This improved product manufacturing time is an advantage for small lots as could be used in a 3D print shop or part to order factory for small business manufacturing [61]. In addition, this improved embodied energy of manufacturing [62,63] if dispersed would provide an advantage over conventional manufacturing and home-based manufacturing [60,64,65]. At the same time, this methodology points the way toward potential 3D printing-based mass production [66] by ganging many print heads to manufacture identical bespoke products simultaneously [67–70]. This would in theory allow scaling up to the limits of the mechanical strength of the gantry materials to add additional nozzles and the stepper motors to move the assembly of hot ends. This would provide an advantage over smaller producers if the lot size is matched with the number of heads of the 3D printer, while enabling rates approaching more traditional mass manufacturing. However, practically, as the lot sized increases and the geographic market for a particular product expands, the embodied energy of transportation reduces the benefits of reduced embodied energy of manufacturing. Future work is need in environmental life cycle analysis (LCA) to optimize the digital manufacturing mode for energy efficiency and emissions.

4.2. Areas of Improvement and Comparison to Other Technologies

Extruders nozzles mounted on the Y0/Y1 controlled gantry (e.g., the primary cross-head gantry) are fixed upon the x-axis, providing limited mobility relative to one another. Specifically, all five extruders are controlled by the same X_D , Y_{0D} , and Y_{1D} commands; thus, equivalent movements are required of the head hot end/nozzle. Multi-head FFF systems utilizing Autodesk Project Escher technology [71], for instance the Titan Robotics Cronus 3D Printer [72], allow for hot end individualized positional movements on X, Y and Z for each respective hot end. Current metal-polymer composites designs required a limiting maximum distance of 55 mm in the X-direction. As a result, this limits the maximum part volume printable on the metal-polymer composite Gigabot. To increase the printable part volume, the extents of the printer would have to be enlarged to accommodate hot end linear spacing greater than 55 mm. Extension of the machine mechanical limits would also enable the operator practical utilization of the X_D directional motor at increased hot end spacing. However, build volume optimization processes (i.e. component orientation and 2D build plate layout) can aid operators in the design of manufacturing process parameters within the machine limits. Specifically, the metal-polymer Gigabot retains the ability to print components with their primary (maximum) linear dimension to be oriented perpendicular to the X-direction on the print bed. Effectively, this requires an increased utilization of Y_{0D} and Y_{1D} for printing as opposed to X_D . Baumers developed an algorithmic methodology promoting densification of available build plate volume [73]. The methodology employs a selection criterion to promote agglomeration of parts in a build volume [73]. The criterion includes part rotation/orientation, part X/Y positioning coordinates, collision checking and total surface area of the part. In practice, the algorithm selects components to be printed and places them in the proper geometrical coordinates such that their centers of mass are as near as possible to their nearest neighbor [73]. Chernov et al. has developed a practical packing algorithm for classical cutting and packing (C&P) problems. The realized application promotes the minimization of scrap loss during fabrication techniques, such as garment manufacturing, sheet metal cutting and furniture manufacturing. The heuristic algorithms are also applicable to 3D packaging efficiency simulations (i.e., cargo shipments and granular media packaging). For the prescribed models, most are commonly used to analyze simplified polygons fixed in a specific orientation denoted as phi-objects [74]. Similar phi-object models are presented in [75,76]. In FFF printing processes, the operator commonly selects the build orientation based on metrics related to print quality, dimensional stability and mechanical properties. Thus, the slicing software (i.e., Slic3r) is responsible for the X/Y orientation of components

to an engineered build plate “density” based on the software algorithms. Thus, while currently developed for non-additive manufacturing processes, Chernov et al.’s methodologies and driving equations could be applied to any metal-polymer composite Gigabot manufacturing system in an effort to optimize build platform part layout under machine constraints. Furthermore, while these methodologies are to be applied to optimize manufacturing processes due to mechanical constraints, in the context of the metal-polymer Gigabot, there are also significant advantages to be discovered from an embodied energy and total capacity utilization (Table 11) standpoint in regards to multi-head ($\times 5$) printing.

Bowden sheaths are utilized to provide feed stock material to the five hexagon hot ends. Bowden sheaths reduce the amount of weight on the extruder gantry. A reduction in gantry weight, on any printing system, is generally considered to increase the part quality and positional accuracy as there is less momentum shift between various vector paths. This phenomena is most apparent at faster print speeds. Other composite printers readily available in the marketplace (e.g., Mark Forged) use a direct drive system [77]. At the expense of gantry weight, direct drive printers allow for flexible materials to be extruded. Direct drive accomplishes this by locating an extruder drive motor near the extruder hot end, thus providing sufficient pressure and not allowing flexible material strands (e.g., carbon fiber, fiberglass, high strength high toughness (HSHT) fiberglass and Kevlar to bend and/or flex [77]. The developed metal-polymer composite Gigabot is able to utilize a Bowden system for the feeding of aluminum wire by requiring a pre-engineer tool path and proper fixturing to pull and weave wire through the guide pin into a specified layer geometry. However, the manufactured fixturing bracket for the five hot ends increases the gantry mass greatly, relatively to the delta-style Bowden system [78]. Subsequently, maximum print speeds are not fully realized as the excess mass causes the X_D positioning motor to slip and lose calibration during fast vector changes.

4.3. Future Work

The layer-based manufacturing methodology described is adaptable to other material systems beyond metal/polymer composites. For example, designed reinforcement schemes utilizing carbon fiber and/or fiber glass strands potentially increase the printed composites mechanical properties. A metal-polymer composite Gigabot allows for site-specific placement of reinforcement material for localized strengthening mechanisms. The performance effects of carbon fiber and/or fiber glass embedding require further investigation. Specifically, bonding mechanisms and mechanical property verification (e.g., tensile, yield, elongation and stiffness) are required prior to any implementation in engineering applications.

5. Conclusions

This study described an open-source manufacturing technology that enables the manufacturing of polymer-metal composite components by providing free and open source hardware and software. The developed printing systems achieves metal wire embedment into a polymer matrix 3D printed part via a novel weaving and wrapping method using OpenSCAD and parametric coding for customized g-code commands. The results indicate that utilizing a multi-polymer head system for multi-component manufacturing reduces manufacturing time by ~420–438% and provides dimensionally-uniform components throughout all hot ends/extruders. Maximum dimensional deviation occurs in the x dimension with a value of 0.18 mm on extruder E3. Thus, multi-component manufacturing can produce dimensionally-accurate parts for practical engineering applications.

Acknowledgments: The authors would like to thank helpful discussion and technical assistance from S. Snabes, M. Fiedler, B. Wijnen, M. Ohadi and G.C. Anzalone. Financial support was provided by the U.S. Department of Energy Advanced Research Projects Agency-Energy (ARPA-E)/University of Maryland Subaward No. 30353-Z7214003. The views and opinions of the authors herein do not necessarily state or reflect those of the United States Government or any agency thereof. Additionally, the authors wish to thank James Klausner and Geoffrey Short (both of ARPA-E) for their technical insight and discussions that favorably affected the design of our modules and the general approach to the problem.

Author Contributions: John J. Laureto defined the metal-polymer composite Gigabot's operational protocols to perform experiments and developed samples. Joshua M. Pearce proposed the research idea and analyzed the products. All authors wrote and edited the paper.

Conflicts of Interest: The authors declare no conflicts of interest.

References

1. Bowyer, A. 3D printing and humanity's first imperfect replicator. *3D Print. Addit. Manuf.* **2014**, *1*, 4–5. [[CrossRef](#)]
2. Rundle, G. *Revolution in the Making: 3D Printing, Robots and the Future*; Affirm Press: South Melbourne, Australia, 2014.
3. Jones, R.; Haufe, P.; Sells, E.; Iravani, P.; Olliver, V.; Palmer, C.; Bowyer, A. Reprap—The replicating rapid prototype. *Robotica* **2011**, *29*, 177–191. [[CrossRef](#)]
4. Sells, E.; Bailard, S.; Smith, Z.; Bowyer, A.; Olliver, V. RepRap: The replicating rapid prototyper-maximizing customizability by breeding the means of production. In *Handbook of Research in Mass Customization and Personalization*; Pillar, F.T., Tseng, M.M., Eds.; World Scientific: Hackensack, NJ, USA, 2009; Volume 1, pp. 568–580.
5. ASTM F2792-12a. *Standard Terminology for Additive Manufacturing Technologies*; ASTM International: West Conshohocken, PA, USA, 2012.
6. Wittbrodt, B.; Pearce, J. M. The effects of PLA color on material properties of 3D printed components. *Addit. Manuf.* **2015**, *8*, 110–116. [[CrossRef](#)]
7. Tymrak, B. M.; Kreiger, M.; Pearce, J. M. Mechanical properties of components fabricated with open-source 3D printers under realistic environmental conditions. *Mater. Des.* **2014**, *58*, 242–246. [[CrossRef](#)]
8. Lanzotti, A.; Grasso, M.; Staiano, G.; Martorelli, M. The impact of process parameters on mechanical properties of parts fabricated in PLA with an open-source 3D printer. *Rapid Prototyp. J.* **2015**, *21*, 604–617. [[CrossRef](#)]
9. Afrose, M.F.; Masood, S.H.; Iovenitti, P.; Nikzad, M.; Sbarski, I. Effects of part build orientations on fatigue behaviour of FDM-processed PLA material. *Prog. Addit. Manuf.* **2015**, *1*, 1–8. [[CrossRef](#)]
10. Tanikella, N.G.; Wittbrodt, B.; Pearce, J.M. Tensile Strength of Commercial Polymer Materials for Fused Filament Fabrication 3D Printing. Unpublished work.
11. Kasture, P.V.; Deole, P.; Irwin, J.L. Case Study Using Open Source Additive Manufacturing (AM) Technology for Improved Part Function. In Proceedings of the ASME 2015 International Mechanical Engineering Congress and Exposition, Houston, TX, USA, 13–19 November 2015.
12. Laureto, J.; Tomasi, J.; King, J.A.; Pearce, J.M. Thermal Properties of 3D Printed Polylactic Acid–Metal Composites. *Prog. Addit. Manuf.* **2017**, 1–15. [[CrossRef](#)]
13. Sugavaneswaran, M.; Arumaikkannu, G. Analytical and experimental investigation on elastic modulus of reinforced additive manufactured structure. *Mater. Des.* **2015**, *66*, 29–36. [[CrossRef](#)]
14. Duigou, A.L.; Castro, M.; Bevan, R.; Martin, N. 3D printing of wood fibre biocomposites: From mechanical to actuation functionality. *Mater. Des.* **2016**, *96*, 106–114. [[CrossRef](#)]
15. Taboas, J.M.; Maddox, R.D.; Krebsbach, P.H.; Hollister, S.J. Indirect solid free form fabrication of local and global porous, biomimetic and composite 3D polymer-ceramic scaffolds. *Biomater.* **2003**, *24*, 181–194. [[CrossRef](#)]
16. Seitz, H.; Rieder, W.; Irsen, S.; Leukers, B.; Tille, C. Three-dimensional printing of porous ceramic scaffolds for bone tissue engineering. *J. Biomed. Mater. Res.* **2005**, *74*, 782–788. [[CrossRef](#)] [[PubMed](#)]
17. Habraken, W.J.E.M.; Wolke, J.G.C.; Jansen, J.A. Ceramic composites as matrices and scaffolds for drug delivery in tissue engineering. *Adv. Drug Deliv. Rev.* **2007**, *59*, 234–248. [[CrossRef](#)] [[PubMed](#)]
18. Liu, X.; Ma, P.X. Polymeric Scaffolds for Bone Tissue Engineering. *Ann. Biomed. Eng.* **2004**, *32*, 477–486. [[CrossRef](#)] [[PubMed](#)]
19. Da Silva, J.R.C.; da Fonsêca, G.F.G.; de Andrade, M.M. Mechanical tests in thermoplastic elastomers used in 3D printers for the construction of hand prostheses. In Proceedings of the 2014 Pan American Health Care Exchanges (PAHCE), Brasilia, Brazil, 7–12 April 2014; pp. 1–6.

20. Trachtenberg, J.E.; Mountziaris, P.M.; Miller, J.S.; Wettergreen, M.; Kasper, F.K.; Mikos, A.G. Open-source three-dimensional printing of biodegradable polymer scaffolds for tissue engineering. *J. Biomed. Mater. Res.* **2014**, *102*, 4326–4335. [[CrossRef](#)]
21. Wong, J.Y.; Pfahl, A.C. 3D Printing of Surgical Instruments for Long-Duration Space Missions. *Aviat. Space Environ. Med.* **2014**, *85*, 758–763. [[CrossRef](#)] [[PubMed](#)]
22. Dimas, L.S.; Bratzel, G.H.; Eylon, I.; Buehler, M.J. Tough Composites Inspired by Mineralized Natural Materials: Computation, 3D printing, and Testing. *Adv. Funct. Mater.* **2013**, *23*, 4629–4638. [[CrossRef](#)]
23. Chia, H.N.; Wu, B.M. Recent advances in 3D printing of biomaterials. *J. Biol. Eng.* **2015**, *9*. [[CrossRef](#)] [[PubMed](#)]
24. Espalin, D.; Muse, D.W.; MacDonald, E.; Wicker, R.B. 3D Printing multifunctionality: structures with electronics. *Int. J. Adv. Manuf. Technol.* **2014**, *72*, 963–978. [[CrossRef](#)]
25. Serra, T.; Planell, J.A.; Navarro, M. High-resolution PLA-based composite scaffolds via 3-D printing technology. *Acta Biomaterialia* **2013**, *9*, 5521–5530. [[CrossRef](#)] [[PubMed](#)]
26. Ma, R.R.; Belter, J.T.; Dollar, A.M. Deposition Manufacturing: Design strategies for multimaterial mechanisms via Three-Dimensional printing and material deposition. *J. Mech. Robot.* **2015**, *7*, 021002.
27. Frazier, W.E. Metal Additive Manufacturing: A Review. *J. Mater. Eng. Perform.* **2014**, *23*, 1917–1928. [[CrossRef](#)]
28. Ready, S.; Whiting, G.; Ng, T.N. Multi-Material 3D Printing. *NIP Digit. Fabr. Conf.* **2014**, *2014*, 120–123.
29. Anzalone, G.C.; Zhang, C.; Wijnen, B.; Sanders, P.G.; Pearce, J.M. A Low-Cost Open-Source Metal 3-D Printer. *IEEE Access* **2013**, *1*, 803–810.
30. Haselhuhn, A.S.; Wijnen, B.; Anzalone, G.C.; Sanders, P.G.; Pearce, J.M. In situ formation of substrate release mechanisms for gas metal arc weld metal 3-D printing. *J. Mater. Process. Technol.* **2015**, *226*, 50–59. [[CrossRef](#)]
31. Haselhuhn, A.S.; Gooding, E.J.; Glover, A.G.; Anzalone, G.C.; Wijnen, B.; Sanders, P.G.; Pearce, J.M. Substrate Release Mechanisms for Gas Metal Arc Weld 3D Aluminum Metal Printing. *3D Print. Addit. Manuf.* **2014**, *1*, 204–209. [[CrossRef](#)]
32. Haselhuhn, A.S.; Buhr, M.W.; Wijnen, B.; Sanders, P.G.; Pearce, J.M. Structure-property relationships of common aluminum weld alloys utilized as feedstock for GMAW-based 3-D metal printing. *Mater. Sci. Eng.* **2016**, *673*, 511–523. [[CrossRef](#)]
33. Ding, D.; Pan, Z.; Cuiuri, D.; Li, H. Wire-feed additive manufacturing of metal components: technologies, developments and future interests. *Int. J. Adv. Manuf. Technol.* **2015**, *81*, 465–481. [[CrossRef](#)]
34. Wijnen, B.; Anzalone, G.C.; Haselhuhn, A.S.; Sanders, P.G.; Pearce, J.M. Free and open-source control software for 3D motion and processing. *J. Open Res. Softw.* **2015**, *4*. [[CrossRef](#)]
35. Laureto, J.; Dessiatoun, S.; Ohadi, M.; Pearce, J. Open Source Laser Polymer Welding System: Design and Characterization of Linear Low-Density Polyethylene Multilayer Welds. *Machines* **2016**, *4*, 14. [[CrossRef](#)]
36. Anzalone, G.C.; Wijnen, B.; Pearce, J.M. Multi-material additive and subtractive prosumer digital fabrication with a free and open-source convertible delta RepRap 3-D printer. *Rapid Prototyp. J.* **2015**, *21*, 506–519. [[CrossRef](#)]
37. Pearce, J.M. Applications of open source 3D printing on small farms. *Org. Farming* **2015**, *1*, 19–35.
38. Nilsiam, Y.; Haselhuhn, A.; Wijnen, B.; Sanders, P.; Pearce, J. Integrated Voltage—Current Monitoring and Control of Gas Metal Arc Weld Magnetic Ball-Jointed Open Source 3-D Printer. *Machines* **2015**, *3*, 339–351. [[CrossRef](#)]
39. Quan, Z.; Wu, A.; Keefe, M.; Qin, X.; Yu, J.; Suhr, J.; Byun, J.-H.; Kim, B.-S.; Chou, T.-W. Additive manufacturing of multi-directional preforms for composites: opportunities and challenges. *Mater. Today* **2015**, *18*, 503–512. [[CrossRef](#)]
40. Bayless, J.; Chen, M.; Dai, B. Wire embedding 3D printer. 2010. Available online: http://www.reprap.org/mediawiki/images/2/25/SpoolHead_FinalReport.pdf (accessed on 19 April 2017).
41. Shemelya, C.; Cedillos, F.; Aguilera, E.; Espalin, D.; Muse, D.; Wicker, R.; MacDonald, E. Encapsulated Copper Wire and Copper Mesh Capacitive Sensing for 3-D Printing Applications. *IEEE Sens. J.* **2015**, *15*, 1280–1286. [[CrossRef](#)]
42. Kim, C.; Espalin, D.; Cuaron, A.; Perez, M.A.; Lee, M.; MacDonald, E.; Wicker, R.B. Cooperative Tool Path Planning for Wire Embedding on Additively Manufactured Curved Surfaces Using Robot Kinematics. *J. Mech. Robot.* **2015**, *7*, 021003–021010. [[CrossRef](#)]

43. Saari, M.; Cox, B.; Richer, E.; Krueger, P.S.; Cohen, A.L. Fiber Encapsulation Additive Manufacturing: An Enabling Technology for 3D Printing of Electromechanical Devices and Robotic Components. *3D Print. Addit. Manuf.* **2015**, *2*, 32–39. [[CrossRef](#)]
44. Macdonald, E.; Salas, R.; Espalin, D.; Perez, M.; Aguilera, E.; Muse, D.; Wicker, R.B. 3D Printing for the Rapid Prototyping of Structural Electronics. *IEEE Access* **2014**, *2*, 234–242. [[CrossRef](#)]
45. Francia, D.; Caligiana, G.; Liverani, A.; Frizziero, L.; Donnici, G. PrinterCAD: A QFD and TRIZ integrated design solution for large size open moulding manufacturing. *Int. J. Interact. Des. Manuf.* **2017**, *1*–14. [[CrossRef](#)]
46. Re:3D. Available online: <http://shop.re3d.org/> (accessed on 19 April 2017).
47. OpenSCAD. Available online: <http://www.openscad.org/> (accessed on 19 April 2017).
48. Open Science Framework. Available online: <https://osf.io/jvhqt/> (accessed on 19 April 2017).
49. GNU General Public License. Available online: <http://www.gnu.org/licenses/gpl-3.0.en.html> (accessed on 19 April 2017).
50. MOST Gigabot. Available online: http://www.appropedia.org/Franklin_Firmware_on_GigabotHX:MOST (accessed on 19 April 2017).
51. IC3D Digital Platform. Available online: <https://www.ic3dprinters.com/index.html> (accessed on 19 January 2017).
52. RAMPS 1.4. Available online: http://reprap.org/wiki/RAMPS_1.4 (accessed on 19 April 2017).
53. Pololu A4988 Stepper Motor Drive Carrier. Available online: <https://www.pololu.com/product/1182> (accessed on 19 April 2017).
54. Arduino Mega Board 2560. Available online: <https://www.arduino.cc/en/Main/ArduinoBoardMega2560> (accessed on 19 April 2017).
55. KiCad-PcbNew. Available online: <http://kicad-pcb.org/discover/pcbnew/> (accessed on 19 April 2017).
56. Slic3r. Available online: <http://slic3r.org/> (accessed on 19 April 2017).
57. eSUN-PETG Technical Data Sheet. Available online: <http://www.esun3d.net/products/176.html> (accessed on 19 April 2017).
58. Gizmo Dorks—PP Technical Data Sheet. Available online: <http://gizmodorks.com/polypropylene-3d-printer-filament/> (accessed on 19 April 2017).
59. Cura. Available online: <https://ultimaker.com/en/products/cura-software> (accessed on 19 April 2017).
60. Petersen, E.; Pearce, J. Emergence of Home Manufacturing in the Developed World: Return on Investment for Open-Source 3-D Printers. *Technologies* **2017**, *5*, 7. [[CrossRef](#)]
61. Laplume, A.; Anzalone, G.C.; Pearce, J.M. Open-source, self-replicating 3-D printer factory for small-business manufacturing. *Int. J. Adv. Manuf. Technol.* **2016**, *85*, 633–642. [[CrossRef](#)]
62. Kreiger, M.; Pearce, J.M. Environmental Impacts of Distributed Manufacturing from 3-D Printing of Polymer Components and Products. *MRS Proc.* **2013**, *1492*, 85–90. [[CrossRef](#)]
63. Megan, K.; Pearce, J.M. Environmental life cycle analysis of distributed three-dimensional printing and conventional manufacturing of polymer products. *ACS Sustain. Chem. Eng.* **2013**, *1*, 1511–1519.
64. Wittbrodt, B.T.; Glover, A.G.; Laureto, J.; Anzalone, G.C.; Oppliger, D.; Irwin, J.L.; Pearce, J.M. Life-cycle economic analysis of distributed manufacturing with open-source 3-D printers. *Mechatron.* **2013**, *23*, 713–726. [[CrossRef](#)]
65. Rayna, T.; Striukova, L. From rapid prototyping to home fabrication: How 3D printing is changing business model innovation. *Technol. Forecast. Soc. Chang.* **2016**, *102*, 214–224. [[CrossRef](#)]
66. Bak, D. Rapid prototyping or rapid production? 3D printing processes move industry towards the latter. *Assembl. Autom.* **2003**, *23*, 340–345. [[CrossRef](#)]
67. Hergel, J.; Lefebvre, S. Clean color: Improving multi-filament 3D prints. *Comput. Graphics Forum* **2014**, *33*, 469–478. [[CrossRef](#)]
68. Ali, M.H.; Mir-Nasiri, N.; Ko, W.L. Multi-nozzle extrusion system for 3D printer and its control mechanism. *Int. J. Adv. Manuf. Technol.* **2016**, *86*, 999–1010. [[CrossRef](#)]
69. Abilgaziyev, A.; Kulzhan, T.; Raissov, N.; Ali, M.H.; Match, W.L.K.; Mir-Nasiri, N. Design and development of multi-nozzle extrusion system for 3D printer. In Proceedings of the 2015 International Conference on Informatics, Electronics & Vision (ICIEV), Fukuoka, Japan, 15–18 June 2015; pp. 1–5.
70. Song, X.; Pan, Y.; Chen, Y. Development of a Low-Cost Parallel Kinematic Machine for Multidirectional Additive Manufacturing. *J. Manuf. Sci. Eng.* **2015**, *137*, 021005–021013. [[CrossRef](#)]

71. Autodesk Project Escher. Available online: <http://projectescher.com/> (accessed on 19 April 2017).
72. Titan Robotics–Cronus 3D Printer. Available online: <http://www.titan3drobotics.com/the-cronus/> (accessed on 19 April 2017).
73. Baumers, M. Economic Aspects of Additive Manufacturing: Benefits, Costs and Energy Consumption. Ph.D. Thesis, Loughborough University, Leicestershire, UK, 2012. Available online: <https://dspace.lboro.ac.uk/dspace-jspui/handle/2134/10768> (accessed on 4 April 2017).
74. Chernov, N.; Stoyan, Y.; Romanova, T. Mathematical model and efficient algorithms for object packing problem. *Comput. Geom.* **2010**, *43*, 535–553. [[CrossRef](#)]
75. Bennell, J.; Scheithauer, G.; Stoyan, Y.; Romanova, T. Tools of mathematical modeling of arbitrary object packing problems. *Ann. Oper. Res.* **2010**, *179*, 343–368. [[CrossRef](#)]
76. Chernov, N.; Stoyan, Y.; Romanova, T.; Pankratov, A. Phi-Functions for 2D Objects Formed by Line Segments and Circular Arcs. *Adv. Oper. Res.* **2012**, *2012*, 26. [[CrossRef](#)]
77. Markforged Composite 3D Printer. Available online: <https://markforged.com/why-markforged/> (accessed on 19 April 2017).
78. MOST Athena Delta—End Effector. Available online: http://www.appropedia.org/Athena_Effector_Assembly (accessed on 19 April 2017).



© 2017 by the authors. Licensee MDPI, Basel, Switzerland. This article is an open access article distributed under the terms and conditions of the Creative Commons Attribution (CC BY) license (<http://creativecommons.org/licenses/by/4.0/>).